

External cavity diode laser as a stable-frequency light source for application in laser cooling of molecules

Xiuxiu Yang (杨秀秀), Yanning Yin (尹燕宁), Xingjia Li (李兴佳), Supeng Xu (徐素鹏), Yong Xia (夏勇)*, and Jianping Yin (印建平)

State Key Laboratory of Precision Spectroscopy, Department of Physics,
East China Normal University, Shanghai 200062, China

*Corresponding author: yxia@phy.ecnu.edu.cn

Received January 12, 2016; accepted May 5, 2016; posted online May 31, 2016

We demonstrate a scheme to use a Littman configuration external cavity diode laser (ECDL) as a stable-frequency light source to stabilize two cw single-mode Ti:sapphire lasers for laser cooling of magnesium fluoride molecules. An ECDL based on the Littman configuration is constructed and stabilized by a digital signal processor system. We stabilize the frequency of our ECDL to ± 0.77 MHz precision over 10 h and the Allan standard deviation reaches 2.6×10^{-11} at an integration time of 10 s. We lock two Ti:sapphire lasers through a transfer cavity, and either laser has a long-term frequency stability of ± 2.5 MHz.

OCIS codes: 140.3425, 140.2020, 020.3320.

doi: 10.3788/COL201614.071403.

The quasi-closed optical cycling transition in some diatomic molecules is formed by only using two or three lasers to address multiple vibrational branches^[1-3]. Direct laser cooling molecules promotes rapid development for the field of cold and ultracold molecules. Ultracold diatomic molecules will open a new chapter for the applications ranging from precision measurement to many-body quantum systems and cold chemistry^[4]. Our ongoing experiment of laser cooling molecules selects the magnesium fluoride (MgF) molecule as a candidate to have the following characteristics^[5]: (1) the $X^2\Sigma^+ - A^2\Pi_{1/2}$ electronic transition of the MgF molecule has highly diagonal Franck-Condon factors; (2) a strong spontaneous emission decay due to the short lifetime (7–8 ns) of its first electronically excited state $A^2\Pi_{1/2}$, and a large scattering force with a light mass; (3) the simple and specific hyperfine structure of the MgF molecule and its small hyperfine splitting due to the electron spin ($S = 1/2$), nuclear rotation, and nuclear spin ($I = 1/2$) interactions for the rotational $N = 1$ energy level of the ground state. Due to the more complex internal structure in an MgF molecule, the laser cooling requires several laser systems. For tunable lasers to have a high resolution and high accuracy, it is customary to lock the laser's frequency to a high-finesse reference cavity (to achieve the narrow linewidths) and then to lock the cavity to an atomic or molecular resonance (which then provides the long-term stability). For the present experiments of laser-cooling molecules, the pulsed molecular beam is produced by a pulsed YAG laser ablation from solid targets, which cannot provide stable saturated absorption spectroscopy to stabilize the cooling and repumping laser frequency. There are two main approaches to stabilizing the long-term stability of laser systems. One is to use a scanning optical cavity to transfer the frequency stabilization of a He-Ne laser to the single-mode tunable laser (such as a diode^[1], dye^[6],

and Ti:sapphire laser^[2]), and the feedback is sent to the piezo actuator of the reference cavity of the laser. A second approach is to stabilize the lasers via optical heterodyne measurements with light from a 100 MHz self-referenced Er-doped fiber comb^[2]. For stabilizing the Ti:sapphire laser frequency, a stabilized He-Ne laser is often served as the reference frequency source owing to its high long-term stability of ± 2 MHz^[6,7]. Nevertheless, it is sensitive to the interference of the surrounding environment, and in the laboratory the mechanical vibration and environmental temperature fluctuation are inevitable, thus He-Ne lasers may not be the best choice for a reference frequency source. By contrast, the frequency-stabilized external cavity diode lasers (ECDLs) that served as the reference frequency source can guard against mechanical and thermal disturbances and get the high long-term stability for Ti:sapphire lasers compared to the stabilized He-Ne lasers.

Compared to other kinds of lasers, ECDLs are a compact, low-cost, handy, and energy-efficient option, amenable to electric high frequency modulation and temperature tuning^[8-12]. ECDLs equipped with gratings are popular with two types of the Littrow^[9-11] and Littman configurations^[12]. As with the Littrow model, the Littman one has a relatively lower efficiency and output power, and overcomes the problems of mode-hopping and output beam angular displacement. Most importantly, the laser linewidth can be narrowed to be a one hundred kHz order of magnitude, or narrower. There are several kinds of frequency stabilization techniques for ECDLs, such as the Zeeman effect method^[13], Fabry-Perot (F-P) cavity method^[14], saturated absorption method^[15], polarization rotated optical feedback method^[16], fluorescence spectrum method^[17] and modulation transfer spectroscopy method^[18].

We construct an ECDL based on the Littman configuration, whose frequency is locked onto the rubidium (Rb) D_2 transition. The frequency stabilization system is based

on a digital signal processor with dependence on a LabVIEW program, in which a software-based phase-sensitive detector (PSD) and a proportional-integral (PI) processor are more simple and flexible than that based on an analog-circuit one^[19,20]. In the experiment, with the simple software, we have stabilized the frequency of the ECDL to a ± 0.77 MHz precision for the long-term stability. Our ECDL has been used as a frequency reference to stabilize two Ti:sapphire lasers for laser cooling of MgF molecules, and either laser has a long-term frequency stability of ± 2.5 MHz.

A collimation tube used for fixing both a laser diode (Sacher SAL-780-100 AR-coated) and a collimation lens is inserted into the round hole of the green block, as sketched in Fig. 1. To control the temperature of the laser diode, a 30 k Ω thermistor and a thermoelectric cooler (TEC) are employed. The thermistor is glued near the laser diode to measure its temperature, and the TEC is below the green block and attached to the fixing stage (purple block in Fig. 1). A holographic diffraction grating (Optometrics 1200 grooves/mm) is glued onto the fixing stage.

Compared to the hardware-based frequency stabilization system, it is apparent that the software-based one in data processing is more flexible with a variety of algorithms and also eliminates the electromagnetic interference that exists in the analog system. Our digital frequency stabilization system is based on the LabVIEW program. In the experiment, to accurately lock the laser frequency on a saturated absorption peak of a Rb atom, the voltage regulation precision applied to the lead zirconate titanate (PZT) should be as high as possible.

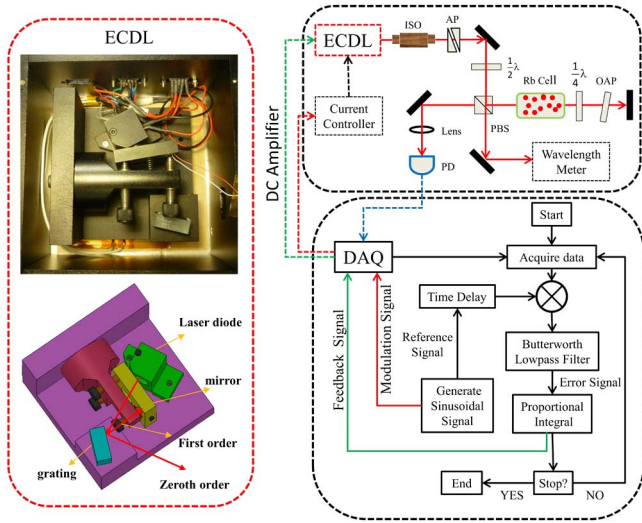


Fig. 1. **Left**, mechanical structure of our Littman cavity ECDL. **Right**, experiment setup for saturated absorption spectroscopy (at the top right) and the flow chart of the laser frequency stabilization (at the bottom right) all based on the LabVIEW program. ISO: optical isolator; AP: anamorphic prisms; $\lambda/2$: half-wave plate; $\lambda/4$: quarter-wave plate; OAP: optical attenuation piece; PD: photodetector; PBS: polarization beam splitter.

Consequently, when the scanning voltage is exterminated, the frequency still stays in the position of the peak. With the visual environment of LabVIEW and the flexible numeric knob, the requirement is easy to achieve; meanwhile, the DC bias signal added in algorithms allows for accurately eliminating the Doppler background.

Figure 1 shows the experiment setup for saturated absorption spectroscopy (at the top right) and the flow chart of the laser frequency stabilization (at the bottom right), which includes the LabVIEW-based PSD and PI servo loop. The flow chart illustrates the control process employed in the LabVIEW program. The DC output signal of the photodetector is sent onto the data acquisition card (DAQ, NI PCI-6259), which acquires the saturated absorption spectroscopy of the Rb atom, as shown in Fig. 2(a). To acquire the error signal, a small sinusoidal signal with a frequency of 10 kHz generated by the LabVIEW program is applied to the current controller, making the laser frequency modulated at 10 kHz. With an appropriate time delay, the sinusoidal signal multiplies with the absorption signal, and then the mixed signal is filtered with an eighth-order Butterworth low pass filter with a bandwidth of 200 kHz; the error signal of one peak is depicted in Fig. 2(b). A proportional and integral processor is necessary to feed an appropriate voltage to the PZT. The feedback voltage can be calculated as

$$V = P e(t) + I \int e(t), \quad (1)$$

where P and I are the proportional and integral values, respectively, $e(t)$ is the error signal, and V is the feedback voltage. With a DC amplifier, the feedback voltage can be amplified by a factor of 20.

The magnitude of the frequency excursion and the drift from the peak can be deduced from the error signal, which

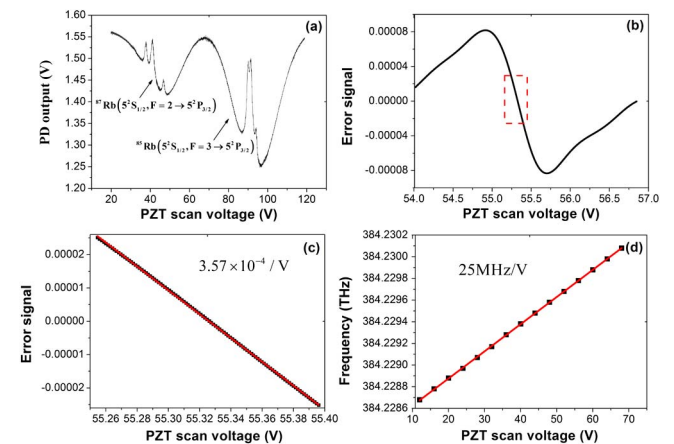


Fig. 2. (a) Saturated absorption spectroscopy of Rb D_2 lines acquired based on the LabVIEW program. (b) The error signal with respect to one peak of ^{85}Rb D_2 lines. (c) and (d) The error signal and the laser frequency as a function of the PZT scan voltage with a slope of $3.57 \times 10^{-4}/\text{V}$ and 25 MHz/V, respectively; the points show the original data and the lines are linear fitted curves to the data.

shows the magnitude and direction of the frequency deviation from the peak. We can find that the error signal is approximated as a linear function near zero, from the data inside the dashed frame of Figs. 2(b), and Fig. 2(c) shows the linear fitted curve to these data with a slope of $k_{\text{slope}} = 3.57 \times 10^{-4}/\text{V}$. In addition, Fig. 2(d) illustrates a conversion between the PZT scan voltage and the laser frequency with a nearly linear response of $\omega_{\text{conversion}} = 25 \text{ MHz/V}$. The error signal is sampled once per 0.1 s for 10 h when the laser frequency is locked, and is shown in Fig. 3(a), from which we can get that all of the error signal samples are within approximately $\Delta_{\text{error}} = \pm 2.5 \times 10^{-5}$ from zero. Three quarters of the error signal samples are within approximately $\Delta'_{\text{error}} = \pm 1.1 \times 10^{-5}$, which is illustrated in Fig. 3(b) showing the Gaussian fitted curve with the FWHM of 2.2×10^{-5} to the statistical frequency counts of the error signal samples. According to the conversion between the error signal and laser frequency, the frequency excursions for these hours are estimated as

$$\frac{\omega_{\text{conversion}}}{k_{\text{slope}}} \times \Delta'_{\text{error}} = \pm 0.77 \text{ MHz}. \quad (2)$$

Therefore, we have stabilized the frequency of our ECDL to $\pm 0.77 \text{ MHz}$, which satisfies the requirement for the stability of the laser frequency in the laser cooling of molecules experiment.

Figure 3(c) is a record of the feedback voltage to the PZT during these hours, which illustrates how the servo loop continuously compensates the fluctuation of the temperature, the current, and the flow of the air to track the peak. In these hours, the feedback voltage comes to maximum of 60 V, which means the laser frequency drifts appropriately 1500 MHz in total according to the conversion between the voltage and laser frequency. The frequency stability can be deduced from the Allan

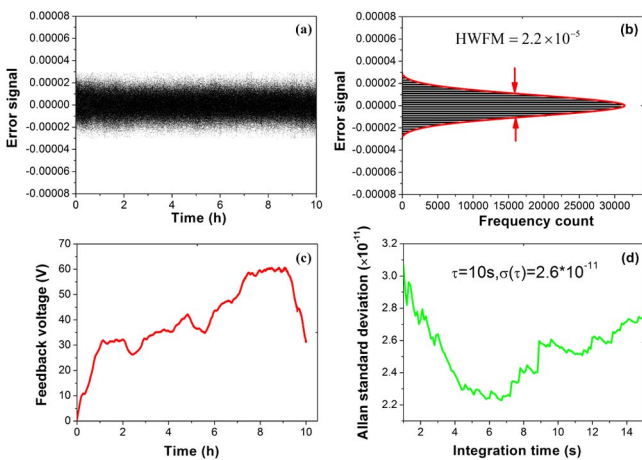


Fig. 3. (a) Error signal sampled for 10 hours. (b) The Gaussian fitted curve to the statistical frequency counts of the error signal samples. (c) The feedback voltage of the PZT via time to show the frequency shift. (d) Frequency stability (Allan standard deviation) of the frequency-stabilized ECDL.

standard deviation of the relative frequency excursions. The Allan deviation is described as

$$\sigma_y^2(\tau) = \frac{1}{2(M-1)} \sum_{i=1}^{M-1} (\overline{y_{i+1}} - \overline{y_i})^2, \quad (3)$$

where σ is the Allan standard deviation, τ is the integration time, M is the number of fractional frequency values, and y_i is the i th of M fractional frequency data averaged over the τ . With the error signals of the Fig. 3(a), Fig. 3(d) gives the Allan standard deviation versus integration time from 1 s to 15 s, from which we get the stability of 2.6×10^{-11} at an integration time of 10 s.

In our ongoing experiment of laser-cooling MgF, we need cw dye lasers or Ti:sapphire lasers with the narrowed linewidth and stabilized frequency serving as the light source; we have demonstrated a frequency stabilization scheme to prepare them. Reference [7] has obtained two Ti:sapphire lasers with a long-term frequency stability of $\pm 2.8 \text{ MHz}$ in which we combine the following two types of locking techniques: “side-of-fringe” and transfer cavity method. Here, we utilize our home-made ECDL in place of the He-Ne laser to serve as the reference frequency source and the experimental setup is depicted in Fig. 4. Both lasers are commercial Ti:sapphire lasers (Matisse TS) that have a free-running frequency drift of $>600 \text{ MHz}$. To stabilize their frequency and narrow their linewidth, we first lock them to their respective reference cells with a free spectral range (FSR) of 600 MHz and atypical finesse of 15 to 20 via a “side-of-fringe” scheme. Owing to the interference of the temperature fluctuation and piezo actuator relaxation to the reference cells, its frequency stability still has a drift of $\sim 74 \text{ MHz/h}$. However, we can suppress this interference to preserve the length of each reference cell as a constant via a transfer cavity method. As sketched in Fig. 4, the transfer cavity is a confocal cavity (Toptica FPI100) with a FSR of 1.0 GHz and a finesse of 400; an triangular wave is applied to the PZT attached to

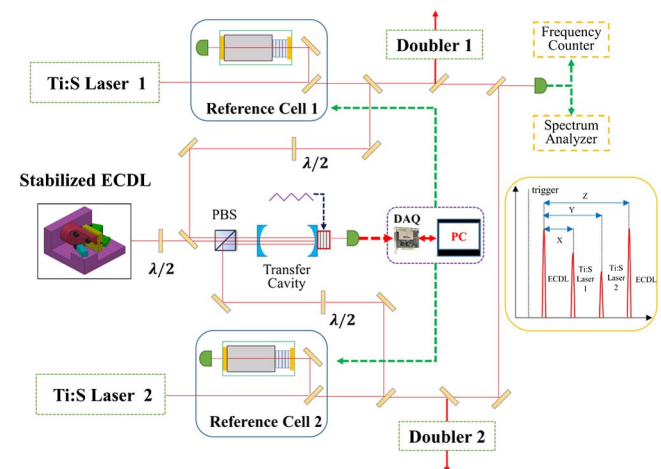


Fig. 4. Experimental setup for Ti:sapphire (Ti:S) laser stabilization.

one cavity mirror scanning its length to obtain the transmission peak of the master and slave lasers. The stabilized ECDL beam is transmitted into the transfer cavity and its transmission signal is being sent through a built-in photo-detector onto a DAQ (NI PCI-6259) and processed by a PC with a LabVIEW program (see the inset of Fig. 4). Owing to the temperature fluctuation and piezo actuator relaxation, the location of the ECDL transmission peak is not stationary, hence we should lock it via an error signal from the deviation between the real-time location and the locking point, in which a feedback voltage is added to the triangular wave scanning the transfer cavity to realize this goal. After locking the transfer cavity, two reference cells can be locked onto it to realize the long-term stability of two Ti:sapphire lasers. Just like what we do to stabilize ECDL, two lasers are processed by a similar procedure in which our program first computes the spacing of two adjacent ECDL peaks (denoted Z here) and the spacing between the first Ti:sapphire laser peak and the first ECDL peak (denoted X here), and feeds back a voltage to the first reference cell locking its length according to the deviation between the ratio X/Z and a selected constant between 0 and 1. For another laser, the above steps are repeated to lock the Y/Z onto another chosen constant in order to realize its long-term stability. With this feedback, the stability of our stabilized ECDL can be transferred to the Ti:sapphire lasers.

As shown in Fig. 4, to obtain the absolute frequency stability of the Ti:sapphire lasers, the beat note between them are recorded and the result is depicted in Fig. 5. As sketched in Fig. 5, the frequency of the beat note in more than one h recorded by a frequency counter with an integration time of 100 ms indicates a frequency stability of ± 2.5 MHz. The stability of the frequency-stabilized laser and the beat frequency obeys

$$\sigma_1(\tau) = \sigma_2(\tau) = \frac{1}{\sqrt{2}}\sigma_{\text{tot}}(\tau), \quad (4)$$

where τ is the integration time and $\sigma_{\text{tot}}(\tau)$ represents the Allan standard deviation of the beat frequency, while $\sigma_1(\tau)$ as well as $\sigma_2(\tau)$ represents the Allan standard deviation of either laser frequency. With Eqs. (3) and (4), we find the absolute frequency stability of either

Ti:sapphire laser is 1.5×10^{-10} with an integration time of 1 s. Compared with the stability of 2.6×10^{-11} of the ECDL, the result for the Ti:sapphire laser becomes worse taking into account the interference of the temperature fluctuation and piezo actuator relaxation to the reference cells and transfer cavity. In addition, the speed of the feedback to the reference cells and transfer cavity limits the short-term stability. The beat note also indicates that the linewidth of the Ti:sapphire laser is 6 kHz because the linewidth is determined by the reference cell module no matter whether the Ti:sapphire laser is locked onto the transfer cavity or not and the stabilized frequency source can only optimize the long-term stability of the Ti:sapphire laser.

Compared with the result in Ref. [7], we can find that the new result is a little better. Here, the modulated frequency and intensity of ECDL limits the stability of the Ti:sapphire laser because the position and intensity of the ECDL transmission peak in the transfer cavity contain the modulation signal. Maybe, using the Zeeman effect method with the same digital signal processor system, we can obtain a better result because the output laser is without the modulation signal.

Although the evaluation of the laser frequency excursion from the error signal is simple and convenient, taking into account the variations of the Doppler broadening shape, the frequency where the error signal equals zero is uncertain and also the slope of the error signal may change. Besides the power of pump and probe light making a difference in the Doppler broadening shape, it is also dependent on the ambient temperature of Rb cell. Consequently, to optimize the reliability of our results in the following work, we should begin with an additional temperature control of Rb cell.

In conclusion, we construct an ECDL based on the Littman configuration and also demonstrate a robust frequency-stabilized laser based on a digital signal processor that extracts the error signal to directly analyze the long-term and short-term stability of the laser. In a free running mode, the laser frequency drifts approximately 1500 MHz within 10 h. We stabilize the frequency of the ECDL to a ± 0.77 MHz precision over 10 h and the short-term frequency stability reaches 2.6×10^{-11} at an integration time of 10 s. Our ECDL is used as a frequency reference to stabilize two Ti:sapphire lasers for laser cooling of MgF molecules, and either laser has a long-term frequency stability of ± 2.5 MHz. In the following work, we will apply an additional temperature control to the ambient temperature of our ECDL besides to the laser diode.

Until now, the robust and versatile solutions demonstrated for locking the tunable laser systems (such as diode^[4], dye^[6] or Ti:sapphire^[7]) are more accessible and particularly useful for applications in the laser cooling of molecules, which need linewidth-narrowed and frequency-stabilized lasers.

This work was supported by the National Natural Science Foundation of China (Nos. 11374100,

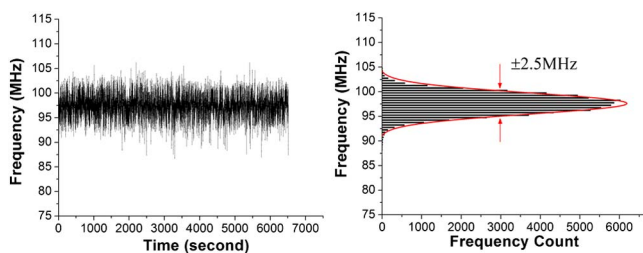


Fig. 5. Frequency of the beat note in more than one h , recorded using a frequency counter with an integration time of 100 ms. The Gaussian fitted curve indicates a frequency stability of ± 2.5 MHz.

91536218, and 11274114) and the Natural Science Foundation of Shanghai Municipality (No. 13ZR1412800).

References

1. E. S. Shuman, J. F. Barry, D. R. Glenn, and D. DeMille, *Phys. Rev. Lett.* **103**, 223001 (2009).
2. M. T. Hummon, M. Yeo, B. K. Stuhl, A. L. Collopy, Y. Xia, and J. Ye, *Phys. Rev. Lett.* **110**, 143001 (2013).
3. V. Zhelyazkova, A. Cournol, T. E. Wall, A. Matsushima, J. J. Hudson, E. A. Hinds, M. R. Tarbutt, and B. E. Sauer, *Phys. Rev. A* **89**, 053416 (2014).
4. L. D. Carr, D. DeMille, R. V. Krems, and J. Ye, *New J. Phys.* **11**, 055049 (2009).
5. D. P. Dai, Y. Xia, Y. F. Fang, L. Xu, Y. N. Yin, X. J. Li, X. X. Yang, and J. P. Yin, *J. Phys. B* **48**, 085302 (2015).
6. D. P. Dai, Y. Xia, Y. N. Yin, X. X. Yang, Y. F. Fang, X. J. Li, and J. P. Yin, *Opt. Express* **22**, 28645 (2014).
7. Y. N. Yin, Y. Xia, X. J. Li, X. X. Yang, S. P. Xu, and J. P. Yin, *Appl. Phys. Express* **8**, 092701 (2015).
8. C. E. Wieman and L. Hollberg, *Rev. Sci. Instrum.* **62**, 1 (1991).
9. T. Zhou, X. Qi, Q. Wang, W. Xiong, J. Duan, X. Zhou, and X. Chen, *Chin. Opt. Lett.* **8**, 496 (2010).
10. S. Dutta, D. S. Elliott, and Y. P. Chen, *Appl. Phys. B* **106**, 629 (2012).
11. N. Ruhnke, A. Müller, B. Eppich, M. Maiwald, B. Sumpf, G. Erbert, and G. Tränkle, *Opt. Lett.* **39**, 3794 (2014).
12. S. E. Park, T. Y. Kwon, E. J. Shin, and H. S. Lee, *IEEE Trans. Instrum. Meas.* **52**, 280 (2003).
13. K. L. Corwin, Z. T. Lu, C. F. Hand, R. J. Epstein, and C. E. Wieman, *Appl. Opt.* **37**, 3295 (1998).
14. A. Schoof, J. Grünert, S. Ritter, and A. Hemmerich, *Opt. Lett.* **26**, 1562 (2001).
15. W. Ma, L. Dong, W. Yin, C. Li, and S. Jia, *Chin. Opt. Lett.* **2**, 486 (2004).
16. Y. G. Sun, F. Wei, Z. R. Dong, D. J. Chen, H. W. Cai, and R. H. Qu, *Opt. Express* **22**, 15757 (2014).
17. Y. Long, Z. Xiong, X. Zhang, M. Zhang, B. Lü, and L. He, *Chin. Opt. Lett.* **12**, 021401 (2014).
18. Y. Han, S. Guo, J. Wang, H. Liu, J. He, and J. Wang, *Chin. Opt. Lett.* **12**, 121401 (2014).
19. T. Ahola, J. P. Hu, and E. Ikonen, *Rev. Sci. Instrum.* **69**, 1934 (1998).
20. G. Koch, *Opt. Eng.* **42**, 1690 (2003).